ACS Synthetic Biology
Cite This: ACS Synth. Biol. 2018, 7, 1629−1639
Research Article
pubs.acs.org/synthbio

Protein-Scaffold Directed Nanoscale Assembly of T Cell Ligands: Artificial Antigen Presentation with Defined Valency, Density, and Ratio

Mason R. Smith, Stephanie V. Tolbert, and Fei Wen*

Department of Chemical Engineering, University of Michigan, Ann Arbor, Michigan 48109, United States

Supporting Information

ABSTRACT: Tuning antigen presentation to T cells is a critical step in investigating key aspects of T cell activation. However, existing technologies have a limited ability to control the spatial and stoichiometric organization of T cell ligands on 3D surfaces. Here, we developed an artificial antigen presentation platform based on protein scaffold-directed assembly that allows fine control over the spatial and stoichiometric organization of T cell ligands on a 3D yeast cell surface. Using this system, we observed that the T cell activation threshold on a 3D surface is independent of peptide-major histocompatibility complex (pMHC) valency but instead is determined by the overall pMHC surface density. When intercellular adhesion molecule 1 (ICAM-1) was coassembled with pMHC, it enhanced antigen recognition sensitivity by 6-fold. Further, T cells responded with different magnitudes to varying ratios of pMHC and ICAM-1 and exhibited a maximum response at a ratio of 15% pMHC and 85% ICAM-1, introducing an additional parameter for tuning T cell activation. This protein scaffold-directed assembly technology is readily transferrable to acellular surfaces for translational research as well as large-scale T-cell manufacturing.

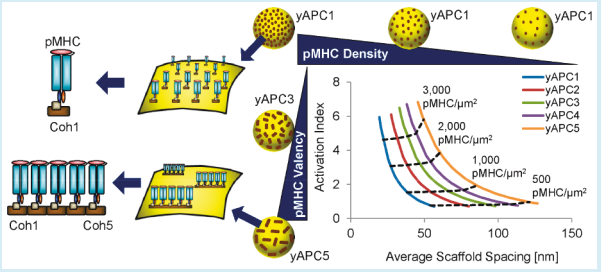

KEYWORDS: *protein assembly, artificial antigen presentation, T cell activation, pMHC, cancer immunotherapy, protein engineering*

T cells are important immune cells for fighting infections and cancers, and as such, T-cell-based immunotherapy offers curative potential in the treatment of many immune-modulating diseases.[1−5] In nature, T cells are activated by binding peptide-major histocompatibility complex (pMHC) and costimulatory molecules displayed on the surface of antigen presenting cells (APCs). These T cell ligands form complex multicomponent assemblies with both micro- and nanoscale organization. The spatial and stoichiometric organization of these assemblies promotes T cell expansion and helps determine T cell phenotype and function.[6,7] Therefore, identifying the spatial and stoichiometric parameters of T cell ligand assemblies that promote robust T cell activation is critical for revealing molecular insights for generating high-quality immunotherapeutic T cells.

A variety of artificial antigen presentation systems have been developed to control the spatial organization of T cell ligands including modified fluid lipid bilayers[8−12] and patterned coverslips.[12−14] Nanolithographic patterning of TCR ligands (e.g., anti-CD3, anti-TCR, and pMHC) on glass coverslips has been used to determine a minimum pMHC surface density of 90−140 pMHC/μm^2 for T cell activation.[15,16] Above this threshold, T cell response can be fine-tuned by controlling the global TCR-ligand surface density.[16−18] The nanoscale organization of TCR-ligands can be quantified as TCR-ligand valency and has also been shown to affect T cell activation.[19−23] When two soluble pMHC molecules are cross-linked by a peptide linker, T cell activation is inversely correlated with the linker length (5−9 nm).[19] Other studies demonstrated that T cell activation can be further enhanced several-fold by increasing the degree of valency of soluble TCR ligands up to 10 for anti-CD3[20] and up to 300 for pMHC.[21] Despite reports that soluble multivalent pMHC complexes enhance T cell activation, it is unclear if T cells respond similarly to surface-bound multivalent pMHC.[24] Given that class II pMHC arrives at the plasma membrane of dendritic cells in sub-100 nm microclusters[25] and TCRs on resting T cells are similarly aggregated,[26] there is reason to believe that surface-bound multivalent pMHC may enhance T cell activation through avidity effects.

The overwhelming majority of artificial antigen presentation systems that allow the nanoscale tuning of TCR ligand organization are 2D. Although 2D systems are powerful research platforms amenable to elegant imaging and signaling studies, their planar geometry represents a significant departure from 3D cell−cell interactions in nature. For example, planar systems provide sustained interfacial contact between T cells and a relatively unidirectional antigen-presenting surface, whereas 3D cell−cell interactions do not. In addition, 2D artificial antigen presentation systems may have limited scalability in T cell manufacturing due to their lower antigen-presentation surface area per unit than 3D systems. Most

Received: March 19, 2018
Published: May 7, 2018

DOI: 10.1021/acssynbio.8b00119
ACS Synth. Biol. 2018, 7, 1629−1639

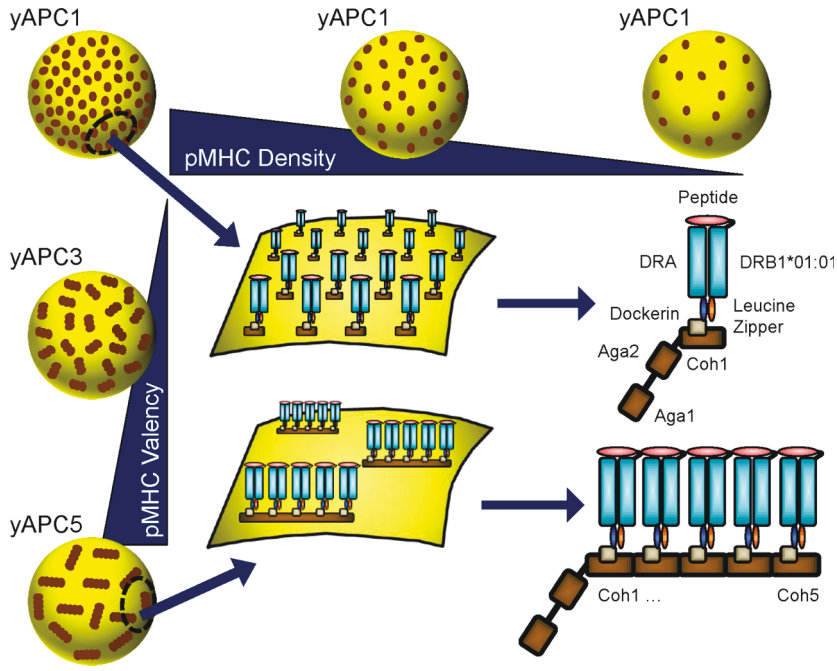

Figure 1. Schematic depicting yAPC system assembly and tunability. yAPC was engineered to accommodate pMHC with valency between 1 (yAPC1) and 5 (yAPC5). Scaffold spacing and the corresponding global pMHC surface density can be tuned to generate yAPCs with a broad range of pMHC surface densities. pMHC was expressed as a heterodimer stabilized by a leucine zipper. The N-terminus of the pMHC β-chain (DRB1*01:01) was fused to the peptide. The C-terminus of the pMHC alpha chain (DRA) was fused to a dockerin-domain from *C. thermocellum*, which specifically associates with corresponding cohesin domains (Coh1−Coh5) from *C. thermocellum* expressed as yeast-surface displayed, Aga2-fused cohesin scaffolds.

current large-scale *ex vivo* T cell activation is performed in bioreactors using anti-CD3/anti-CD28-coated beads. Recent advances in the design of patchy particles[27,28] have enabled the regular patterning of 3D surfaces; however, the resolution of this approach is currently limited to ~3 μm diameter ($1/6^{th}$ the diameter of the microsphere)[27] patches. This patterning resolution is too coarse to probe how T cells respond to nanoscale ligand organization.

In addition to controlling the spatial organization of T cell ligands, artificial antigen presentation systems have also been designed to control the composition of different T cell ligands. In contrast to the aforementioned planar systems, the ones designed to control the composition of costimulatory and adhesion molecules during antigen presentation are often cell lines, and thus 3D. Studies have shown that presentation of intercellular adhesion molecule 1 (ICAM-1) by both cells and acellular beads accelerates the production of IL-2 and IFN-γ by $CD4^+$ T cells.[29] Similarly, 4-1BBL presentation on engineered cells has been shown to enhance the expansion of functional $CD8^+$ T cells more effectively than anti-CD28.[30] The presentation of multiple costimulatory molecules such as various combinations of ICAM-1, CD80, CD86, and 4-1BBL further improves T cell proliferation and activation.[31−33] Although insights gained from manipulating costimulatory signals have already been translated to improved clinical designs of therapeutic T cells,[34] most studies to date have focused on simply combining costimulatory/adhesion molecules with little control over their valency or ratio. This is technically challenging on cell surfaces. Even with synthetic systems, this control has thus far been limited to biotin−avidin-based presentation methods such as anti-CD3/anti-CD28-coated beads[35] and stochastically clustered anti-CD3/anti-CD28/anti-LFA-1 on neutravidin anchored in liposomes.[36] Therefore, the extent to which T cell activation can be tuned by simultaneously modulating the stoichiometric ratio and valency of pMHC and adhesion/costimulatory molecules during antigen presentation remains unclear.

Here, we describe a modular artificial antigen presentation system that provides control over the spatial and stoichiometric organization of immunological proteins on a 3D yeast cell surface using protein scaffold-directed assembly. These yeast antigen-presenting cells (yAPCs) enabled for the first time the systematic and quantitative investigation of how nanoscale protein organization on a 3D surface influences T cell activation. This work presents a new strategy for tuning antigen presentation on 3D surfaces by controlling the valency, density, and ratio of T cell ligands. The underlying principle of scaffold-directed assembly based on high affinity protein−protein interactions described here can be readily applied to acellular 3D surfaces, such as polystyrene and magnetic microparticles and hydrogels,[37] greatly expanding its potential applications.

RESULTS AND DISCUSSION

Molecular Design for Patterning Cell Surface with Defined pMHC Valency and Density. pMHC spatial organization can be controlled by manipulating both the occupancy of nanoscale pMHC clusters on a surface (i.e., pMHC valency) and the global pMHC density across the entire surface. For controlling pMHC valency and the global pMHC surface density, yeast cells were engineered to assemble pMHC on surface-displayed multivalent protein scaffolds (Figure 1). Yeast cells were chosen as a model antigen presenting system for their inability to activate T cells *in vitro*[38−40] and the versatile genetic tools available that allow proteins to be displayed on the yeast cell surface.[40−45] Modular cohesin units

DOI: 10.1021/acssynbio.8b00119
ACS Synth. Biol. 2018, 7, 1629−1639

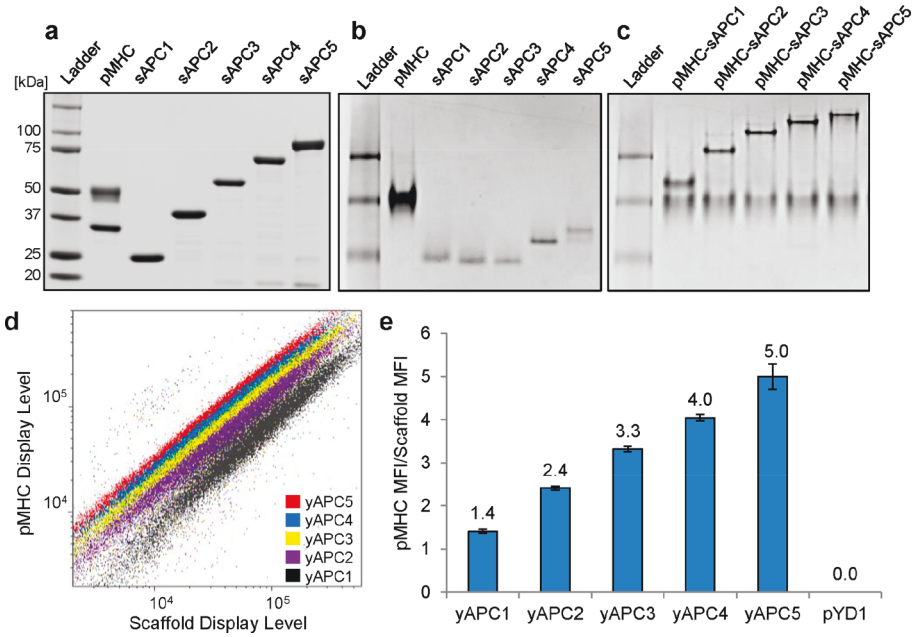

Figure 2. Scaffold-directed assembly of recombinant pMHC achieves expected pMHC valency. (a) SDS-PAGE analysis and (b) native-PAGE analysis of recombinant pMHC and soluble cohesin scaffolds. (c) Native-PAGE shift assay shows dockerin-fused pMHC forming a complex with soluble cohesin scaffolds. Excess pMHC was included to ensure saturation of sAPC scaffold sites. (d) Flow cytometry dot plot showing pMHC display level plotted against the scaffold display level for yeast presenting scaffolds of different valencies. (e) Average number of pMHC per scaffold determined by the ratio of the median fluorescence intensity (MFI) of the bound pMHC and the MFI of the displayed scaffold. Data represent mean ± SD (n = 3). Student's t test indicated any pair within a data set having $p < 0.05$.

from the CipA protein[46] of *Clostridium thermocellum* were recombined to create custom protein scaffolds containing a tunable number of binding sites ranging from one (yAPC1) to five (yAPC5) (Coh1−Coh5 in Figure 1). Cohesin units bind strongly to cognate protein units called dockerins. For organizing pMHC on the yeast-displayed cohesin scaffolds, a cognate dockerin domain[47] from *C. thermocellum* was fused to the alpha-chain of the class II MHC HLA-DR1 (Figure S1A). The pMHC-dockerin fusion allows the protein scaffolds to direct the supramolecular assembly of pMHC on a 3D surface (Figure S1B). pMHC valency is controlled through the number of cohesin units in the protein scaffold. For example, yAPC5 represents a yeast cell displaying protein scaffolds with five cohesin units and therefore presents five pMHC molecules per protein scaffold (Figure 1, bottom right). These multivalent protein scaffolds included an N-terminal Aga2 fusion that forms a disulfide linkage to Aga1 on the yeast cell surface[42] (Figure S1A), allowing the pMHC surface density to be tuned by treating yeast cells with a reducing agent. The protein scaffolds also included a C-terminal V5 epitope tag for detection and molecular quantification.

Protein Scaffold-Directed Assembly of pMHC on a Cell Surface. For verifying the specific binding of dockerin-fused pMHC with cohesin-derived protein scaffolds, soluble forms of the protein scaffolds (sAPCs) and dockerin-fused pMHC were expressed and purified in *E. coli* and insect cells, respectively (Figure 2a). The binding affinity of soluble protein scaffold (sAPC1) and dockerin-fused pMHC was measured using surface plasmon resonance (SPR) and found to be ∼10 nM (Figure S2A). This value is consistent with reported binding affinities for other enzyme−dockerin fusions,[48] suggesting that the fusion of this dockerin to pMHC does not significantly change the affinity of the cohesin−dockerin interaction. Excess dockerin-fused pMHC was incubated with the sAPCs, and complex formation was assessed by a native-PAGE shift assay. The native-PAGE analysis showed a complete shift of each sAPC band accompanied by the appearance of bands with increasing molecular weight in the order of sAPC1 to sAPC5 (Figure 2b and c), indicating complete complex formation between soluble protein scaffolds and dockerin-fused pMHC.

For enabling the assembly of pMHC on the cell surface, yeast cells were transformed with the plasmid encoding the multivalent, Aga2-fused, and V5-tagged protein scaffolds. After protein induction, the transformed yAPC1−yAPC5 were loaded with pMHC and costained with fluorescent antibodies recognizing the pMHC and V5 tag, respectively. The resulting fluorescent signals were then analyzed using flow cytometry to assess the pMHC occupancy of each surface-displayed scaffold (Figure 2d). The average pMHC occupancy of each yAPC scaffold was measured by analyzing the ratio of the pMHC signal to protein scaffold signal. These ratios were then normalized based on the valency of yAPC5. The observed pMHC valency of each protein scaffold construct agreed with its designed stoichiometry, indicating that each cohesin module stably binds a dockerin-fused pMHC (Figure 2e). A yeast cell control presenting no scaffold (pYD1 in Figure 2e) was also incubated with pMHC and analyzed in the same way. No pMHC signal was detectable, indicating that pMHC display is protein-scaffold dependent. The apparent binding affinity between yeast surface-displayed protein scaffolds and pMHC was measured to be 5.70 ± 1.75 nM using a flow-cytometry binding assay (Figure S2B), which was comparable to the binding affinity measured by SPR (10.00 ± 5.06 nM).

T Cell Activation by Multivalent pMHC Assembly. For ensuring the functionality of the multivalent pMHC assembly, the recombinant dockerin-fused pMHC protein was first used to elicit dose-dependent, antigen-specific T cell activation.

DOI: 10.1021/acssynbio.8b00119
ACS Synth. Biol. 2018, 7, 1629−1639

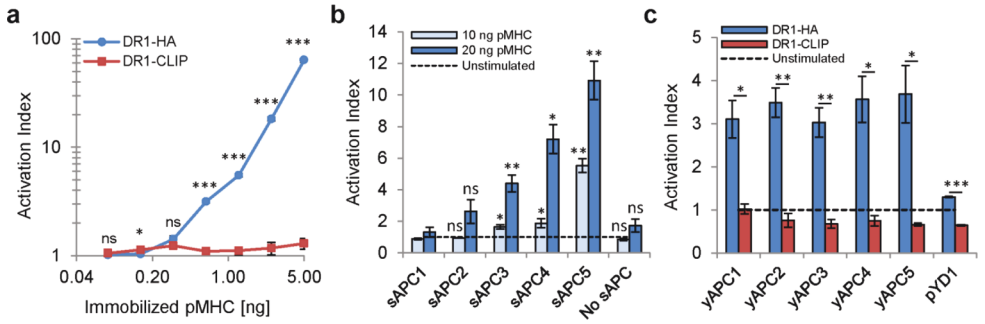

Figure 3. Dockerin-fused pMHC activates HA1.7 T cell hybridoma. (a) T cell response to dockerin-fused pMHC presenting either agonist HA peptide (DR1-HA) or null CLIP peptide (DR1-CLIP) titrated and immobilized in an activation plate. The activation index is the ratio of T cell IL-2 secretion over basal IL-2 signal from unstimulated control. (b) T cell response to soluble pMHC with varying valency assembled on a soluble scaffold (sAPC). Soluble pMHC monomer (no sAPC) was included as a negative control. Activation was performed using either 10 or 20 ng pMHC. Statistical significance was determined with respect to sAPC1. (c) T cell response to dockerin-fused pMHC loaded on yeast displayed scaffolds (yAPC1−yAPC5). yAPC1−yAPC5 loaded with DR1-HA have statistically insignificant difference in activation, but all are statistically different from the negative control pYD1. For a−c, data represent mean ± SD (n = 3, Student's t test, *p < 0.05, **p < 0.01, ***p < 0.001, not significant (ns)).

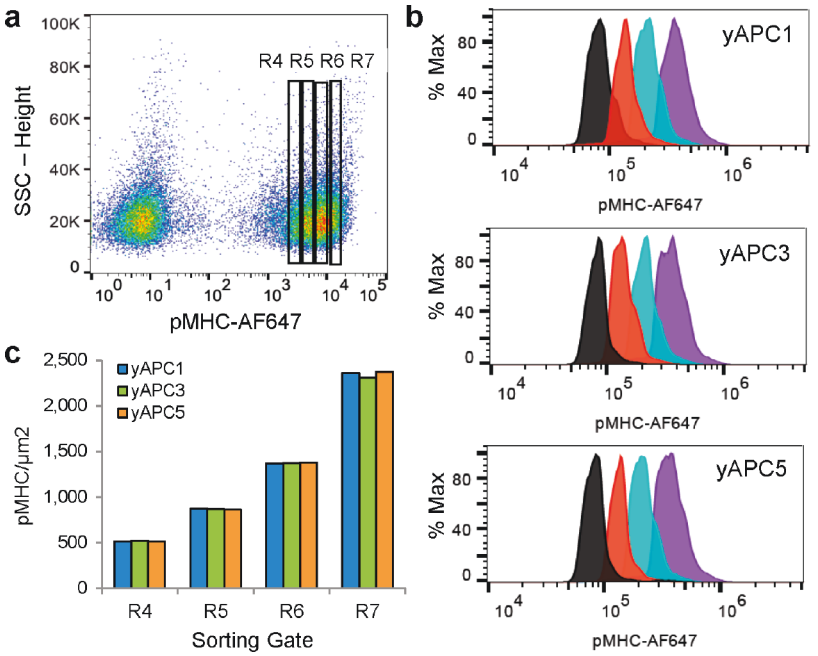

Figure 4. Fluorescence-activated cell sorting (FACS) of yAPC based on pMHC surface density. (a) pMHC-loaded yAPC sorted into populations with different pMHC surface densities (low, R4; high, R7). (b) Sorted yAPC1 (top), yAPC3 (middle), and yAPC5 (bottom) populations analyzed using flow cytometry (left to right: R4, black; R5, red; R6, cyan; R7, purple). (c) Quantification of pMHC surface density of sorted populations. All yAPCs were subjected to the same treatment; yAPC2 and -4 are not shown for simplicity.

Dockerin-fused HLA-DR1 in complex with the influenza antigenic peptide[49] $HA_{306-318}$ (DR1-HA) was used to activate HA1.7 cells, a murine transgenic T cell hybridoma expressing a human α/β TCR that recognizes DR1-HA.[50] Dockerin-fused HLA-DR1 in complex with the invariant chain peptide[51] $CLIP_{87-101}$ (DR1-CLIP) was used as a negative control for antigen specificity. DR1-HA and DR1-CLIP were titrated and adsorbed in a 96-well polystyrene plate and incubated with HA1.7 T cells for activation. After 18 h, IL-2 level in the supernatant was quantified using ELISA. As shown in Figure 3a, HA1.7 T cells responded to immobilized pMHC proteins in an antigen-specific, dose-dependent manner, indicating that the recombinant dockerin-fused pMHC is functional.

Soluble multivalent pMHC has long been known to activate T cells by cross-linking TCRs, whereas soluble monomeric pMHC is incapable of inducing T cell activation.[20,52−54] For validating the pMHC-scaffold assembly scheme and testing the ability of our soluble multivalent pMHC complexes to activate T cells, equal amounts of DR1-HA (pMHC) were loaded on sAPC1−sAPC5, and the soluble pMHC-sAPC complexes were incubated with HA1.7 T cells for activation. An equivalent amount of soluble pMHC monomer (i.e., no sAPC in Figure 3b) was included as a negative control. After 18 h, T cell activation was assessed by quantifying IL-2 in the supernatant using ELISA. In agreement with previous studies, soluble pMHC monomer and pMHC-sAPC1 complexes failed to induce T cell IL-2 secretion (Figure 3b). Moreover, as the pMHC multivalency increased, the degree of T cell activation also increased, suggesting high pMHC multivalency on soluble complexes is more effective at cross-linking TCRs than low pMHC multivalency.

DOI: 10.1021/acssynbio.8b00119
ACS Synth. Biol. 2018, 7, 1629−1639

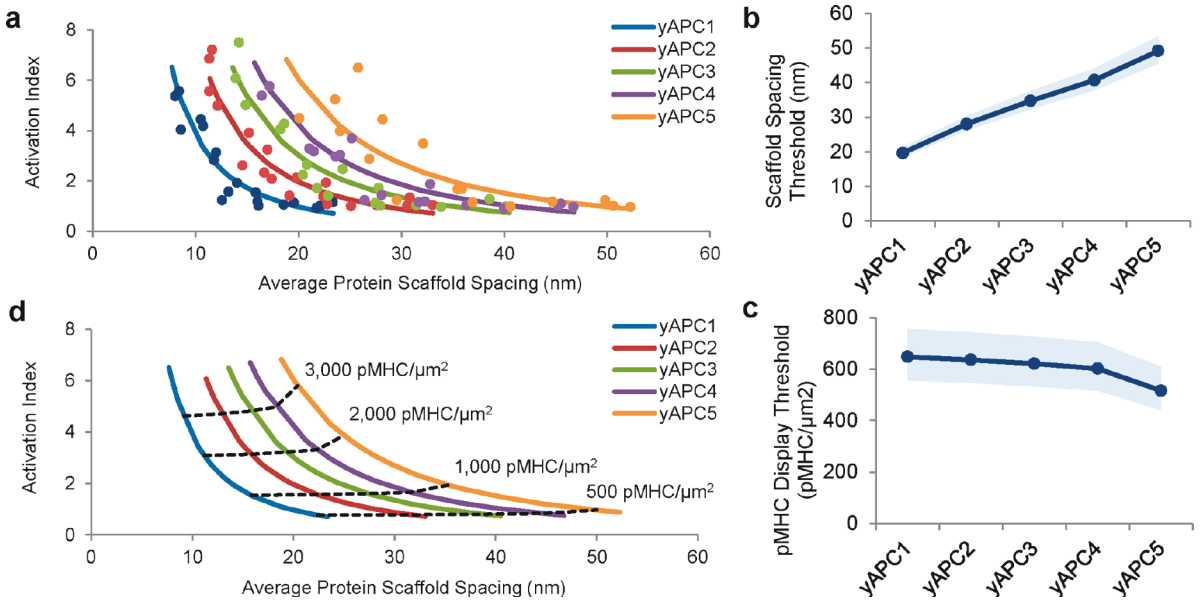

Figure 5. T cell response to changes in global pMHC surface density and local pMHC valency. (a) T cell IL-2 secretion plotted against average scaffold spacing for each yAPC. Regression lines fitted using log−log transformation and linear regression. (b) Using the regressions fitted in (a), the minimum scaffold spacing required for T cell activation plotted for each pMHC valency. The shaded regions represent 95% confidence intervals. (c) Assuming uniform scaffold distribution, the minimum global pMHC density/μm^2 required for T cell activation plotted as a function of pMHC valency. The shaded regions represent 95% confidence interval. (d) Regression of T cell activation index plotted against average scaffold spacing showing lines of constant pMHC surface density.

For further testing the functionality of the protein scaffold-directed pMHC assembly on the yeast cell surface, dockerin-fused DR1-HA and dockerin-fused DR1-CLIP were loaded onto the surface of yAPC1−yAPC5. The resulting yAPCs were then incubated with the HA1.7 T cells at a 10:1 ratio for 18 h, and the IL-2 secretion was quantified using ELISA. Each yAPC construct presenting agonist DR1-HA produced measurable IL-2 secretion, whereas each yAPC construct presenting DR1-CLIP did not (Figure 3c). The yeast cell displaying no protein scaffold (pYD1 in Figure 3c) was also included for both DR1-HA and DR1-CLIP, and neither produced measurable IL-2 secretion. These results suggest that the yeast cells do not nonspecifically activate the T cells, and pMHC organized on yeast-displayed protein scaffolds can induce antigen-specific T cell activation. Interestingly, pMHC valency did not significantly influence the IL-2 secretion by T cells as yAPC1−yAPC5 induced comparable T cell activation after 18 h. This observation could be a result of the natural variation in protein scaffold expression producing similar global pMHC surface densities on each yAPC construct (Figure 2d and Figure S3). Therefore, we next aimed to tune the pMHC surface density on the yAPC constructs.

FACS-Facilitated Tuning of the Global pMHC Surface Density. To control the global pMHC surface density, we stained pMHC-loaded yAPC1−yAPC5 with anti-His fluorescent antibodies and used FACS to isolate yAPC populations with homogeneous pMHC surface densities. As shown in Figure 4a, four gates corresponding to four different pMHC surface densities were used to sort yAPC1−yAPC5. This allowed the same pMHC surface density to be obtained for each pMHC valency. The sorted yAPCs were reanalyzed using flow cytometry to confirm that the pMHC surface density was indeed consistent among yAPC1−yAPC5 (Figure 4b). Fluorescence quantitation beads were used to convert fluorescence intensity into the average pMHC surface density for each yAPC population using eq 1 below (Figure 4c). This process was repeated using yAPCs treated with varying concentrations of tris(2-carboxyethyl)phosphine hydrochloride (TCEP) prior to pMHC loading. TCEP treatment releases a fraction of protein scaffold from the yeast cell surface, broadening the range of possible pMHC surface densities (Figure S4).

Relationship between pMHC Surface Density and Protein Scaffold Spacing. For calculating the pMHC surface density, quantitative flow cytometry was performed using fluorescence quantitation beads. Specifically, yAPCs loaded with pMHC were stained with Alexa Fluor 647-labeled anti-His antibody, and the resulting median fluorescence intensity (MFI) was measured on a flow cytometer. Note that each pMHC molecule has two His tags (Figure S1A). In parallel, fluorescence quantitation beads labeled with known numbers of molecules of equivalent soluble fluorophore (MESF) were analyzed by flow cytometry to convert MFI to the number of pMHC per yAPC surface (Figure S5). The function relating MESF to MFI was determined independently for each experiment. Yeast cells were assumed to be spheres of radius $R = 2\ \mu m$ (ref 55 and Figure S6), and the pMHC surface density was calculated as

$$\text{pMHC surface density} = \frac{A^{*}\text{MFI}_{\text{yAPC}} + B}{2\beta^{*}4\pi R^2} \quad (1)$$

where MFI_{yAPC} represents the MFI of pMHC-loaded yAPC, β represents the degree of fluorescence labeling of the anti-His antibody, and A and B are the slope and intercept, respectively, provided by the MESF vs MFI function shown in Figure S5.

Next, the protein scaffold surface density ρ (i.e., number of protein scaffolds/yAPC surface area) was calculated by dividing the pMHC surface density by the valency of each yAPC construct. Because the protein scaffold was assumed to be randomly distributed across the cell surface (Figure S6), the

DOI: 10.1021/acssynbio.8b00119
ACS Synth. Biol. 2018, 7, 1629−1639

Table 1. T Cell Activation Thresholds Observed for Various Antigen Presentation Systems

TCR ligand	costimulatory ligand	activation readout	patterning technique	spacing threshold	density threshold	ref
pMHC	none	contact area, IL-2 secretion	lithography	100−150 nm	90−140/μm^2	16
aCD3 (OKT3)	aCD28	IL-2 secretion, proliferation	lithography	>150 nm	N/A	17
aCD3 (UCHT1 Fab$_2$)	ICAM-1	pY intensity	lithography	34−69 nm	N/A	18
aCD3 (UCHT1 Fab)	ICAM-1	pY intensity	lithography	100 nm	115/μm^2	15
pMHC	none	IL-2 secretion	scaffold-directed assembly	18−21 nm[a]	550−650/μm^2	this work
pMHC	ICAM-1	IL-2 secretion	scaffold-directed assembly	45−52 nm[a]	92−122/μm^2	this work

[a]Spacing threshold determined for monovalent yAPC1

probability that a protein scaffold is s distance away from its nearest neighbor was calculated using the Poisson distribution $P(s)=2\pi s\rho e^{-\pi\rho s^2}$. Integrating this function from zero to infinity provides the average protein scaffold distance to nearest neighbor (i.e., protein scaffold spacing) $\bar{s}$

$$\bar{s} = \frac{1}{2\sqrt{\rho}} \tag{2}$$

Minimum pMHC Requirement for T Cell Activation. After generating yAPC populations with defined pMHC surface densities and valencies, these well-characterized yAPCs were used to determine how global pMHC surface density, protein scaffold spacing, and pMHC valency influence the T cell activation threshold. T cell activation was assessed by measuring IL-2 in the supernatant after 18 h and plotted as a function of protein scaffold spacing for each pMHC valency (yAPC1−yAPC5) (Figure 5a). In agreement with previous results obtained using 2D systems,[18] monovalent pMHC (i.e., yAPC1) spacing was found to inversely correlate with T cell activation. This inverse correlation was also observed for higher valencies (yAPC2−yAPC5); however, the decrease was more gradual suggesting that increased pMHC valency can compensate for greater protein scaffold spacing.

For interpolating the T cell activation threshold, linear regression was performed on the log−log-transformed data set of activation index and protein scaffold spacing for each yAPC (see Methods for details). Using these regression equations, the protein scaffold spacing at which IL-2 secretion became undetectable (i.e., equal to unstimulated T cells) was determined. This scaffold spacing threshold depended linearly on pMHC valency, ranging from ∼19.6 nm for yAPC1 to ∼49.2 nm for yAPC5 (Figure 5b). The pMHC surface density threshold was then calculated for each yAPC construct using eq 2 and was found to be independent of pMHC valency (Figure 5c and d).

Although we observed that the T cell activation threshold is independent of pMHC valency on the yeast cell surface, at high pMHC surface densities yAPC5 appeared to enhance T cell response (Figure 5d), indicating that pMHC valency may have a secondary effect on T cell activation. Although these results agree with previous studies using ligands anchored on 2D surfaces,[16] they differ from our results using soluble multivalent pMHC complexes (Figure 3b) as well as previous studies,[20] suggesting that T cells respond to TCR ligand valency differently in soluble and surface-bound contexts. This notion is supported by the well-established finding that surface-anchored monomeric pMHC induces T cell activation while soluble monomeric pMHC does not.[20,52−54] It is also possible that the relatively weak relationship between T cell activation and pMHC valency on the yeast cell surface observed in this study is due to the limited pMHC valencies tested. Here, the maximum pMHC valency investigated was five; however, TCRs in nature are clustered at a valency of 7−20 following pMHC engagement.[56] Therefore, further investigation using higher valency scaffolds (e.g., yAPC6, yAPC7, etc.) would be necessary to determine the extent to which pMHC valency on a 3D surface might enhance T cell response.

The observation of a minimum pMHC requirement for T cell activation is consistent with previously published findings using lithographically patterned surfaces.[16] However, the minimum pMHC surface density required for T cell activation on the 3D yAPC surface was significantly higher than that required on 2D planes (Table 1). This discrepancy is likely related to the geometric differences between 2D and 3D systems. In the absence of adhesion and costimulatory molecules, pMHC must function as both the adhesion and stimulatory ligand. The "adhesion" role of pMHC is less important for 2D antigen presentation surfaces as their planar geometry allows for sustained interfacial contact between T cells and the antigen-presenting surface. In contrast, such contact is not assured when T cells are activated by pMHC presented on a 3D surface. Therefore, greater pMHC surface densities are required for antigen presentation on a 3D surface to maintain productive T cell-APC contacts leading to full T cell activation.

Given the abundance of costimulatory and adhesion molecules that participate in T cell activation *in vivo*, we hypothesized that the T cell activation threshold could be reduced by presenting ICAM-1 with pMHC. Further, on the basis of our ability to tune T cell IL-2 secretion by manipulating the spatial organization of pMHC, we believed that T cell IL-2 secretion could also be controlled by manipulating the pMHC-ICAM-1 display ratio. To test these hypotheses, we coassembled pMHC and ICAM-1 on yAPCs.

Protein Scaffold-Directed Coassembly of pMHC and ICAM-1. The extracellular domain of ICAM-1 was fused to the same C-terminal dockerin as the pMHC to allow for coassembly on the yAPC-displayed scaffolds. Dockerin-fused ICAM-1 was analyzed using SDS-PAGE to verify purity and size (Figure S7A,B). The apparent binding affinity of dockerin-fused ICAM-1 for the yAPC cohesin scaffold was measured using a flow cytometry-based binding assay (Figure S7C) and found to be slightly higher than the dockerin-fused pMHC (5.60 nM for the pMHC vs 1.21 nM for ICAM-1). The slightly higher binding affinity of ICAM-1 could be a result of its elongated structure, which may be less prone to steric hindrance than the bulkier heterodimeric pMHC.

The effect of pMHC-ICAM-1 coassembly on T cell activation was assessed by loading various ratios of pMHC and ICAM-1 on unsorted yAPC1, yAPC3, and yAPC5. The fractional occupancy of pMHC and ICAM-1 on the surface of yAPCs was determined by flow cytometry (Figure S8), and the characterized yAPCs were used for T cell activation. For

DOI: 10.1021/acssynbio.8b00119
ACS Synth. Biol. 2018, 7, 1629−1639

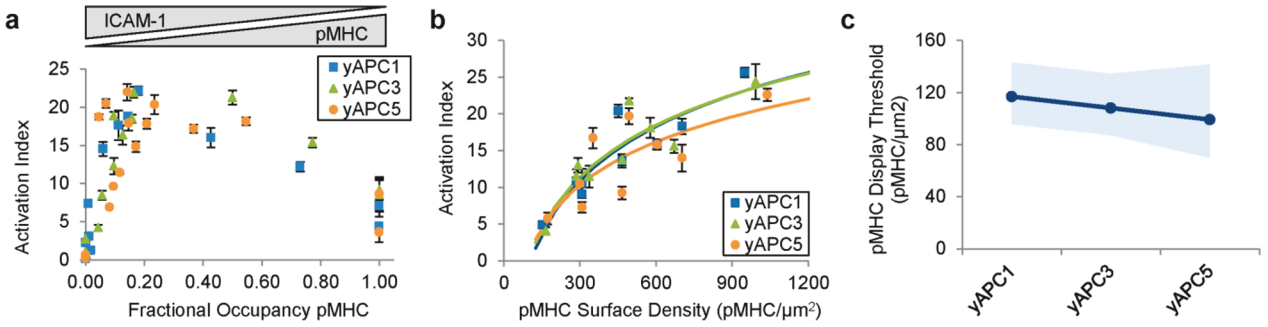

Figure 6. T cell response to yAPC displaying the coassembly of pMHC and ICAM-1. (a) T cell response to unsorted yAPC1, yAPC3, and yAPC5 loaded with various ratios of pMHC and ICAM-1. (b) T cell activation index plotted against global pMHC surface density for sorted yAPC1, yAPC3, and yAPC5 loaded with 85% ICAM-1 and 15% pMHC. The yAPCs were sorted based on fixed overall protein display levels. (c) Solid lines represent regression equations. (c) Minimum pMHC surface density for T cell activation when activated with yAPC1, yAPC3, and yAPC5 presenting 85% ICAM-1 and 15% pMHC. Shaded regions represent 95% confidence intervals.

pMHC-ICAM-1 coassembly, T cell activation increased sharply as the fraction of pMHC increased from 0 to 15% and then gradually decreased up to 100% pMHC (Figure 6a). This optimum assembly ratio of approximately 15% pMHC, 85% ICAM-1 was observed for each yAPC construct, and thus deemed independent of valency (Figure 6a). This optimum suggests that 15% pMHC is sufficient to trigger widespread TCR signaling, which not only initiates T cell activation but also promotes stronger LFA-1-ICAM-1 binding by inducing a conformational change in LFA-1.[57−61] This synergistic interaction led to a ∼3-fold increase in maximum T cell activation despite presenting ∼6-fold less pMHC (Figure 6a vs Figure 5a). It is worth noting that, in addition to mediating intercellular adhesion, ICAM-1-LFA-1 binding has also been shown to sustain intracellular calcium flux that is required for T cell activation.[62] As a result, ICAM-1 exhibits characteristics of both adhesion and costimulatory molecules,[29,63] which might explain the synergy that produced the ∼3-fold increase in T cell activation by the pMHC-ICAM-1 coassemblies.

The T cell activation threshold for the pMHC-ICAM-1 coassembly was determined by first loading yAPC1, yAPC3, and yAPC5 with 15% pMHC and 85% ICAM-1 (Figure S9A). The loaded yAPCs were then stained with a fluorescent anti-His antibody and sorted to isolate homogeneous yAPC populations with defined total ligand surface densities (Figure S9B). T cell activation by these yAPC populations was assessed by measuring IL-2 secretion after 18 h using ELISA and plotted against the global pMHC surface density (Figure 6b). Similar to the results for T cell activation by pMHC alone (Figure 5c), the pMHC surface density threshold for the coassembly did not depend on valency (Figure 6b and c and Figure S10). As we hypothesized, the presence of ICAM-1 reduced the pMHC surface density threshold for T cell activation ∼6-fold to 92−122 pMHC/μm^2, which is comparable to that reported for planar systems (Table 1). This observation supports our hypothesis that sustained intercellular contact is critical for efficient T cell activation and that ICAM-1 mediates this contact more effectively than pMHC alone on 3D antigen-presenting surfaces. In addition to maintaining intercellular contact, fine-tuning the stoichiometric ratio of adhesion and stimulatory T cell ligands may also be useful for directing T cells toward an optimum phenotype. For example, ICAM-1 has been shown to drive $CD4^+$ T cells toward a Th1 phenotype,[64,65] and additional studies of other costimulatory molecules may provide insights that are relevant to the design of future T cell immunotherapeutics and their large-scale manufacture.

In this work, we developed a novel strategy for controlling the valency, surface density, and stoichiometric ratio of T cell ligands on a 3D yeast cell surface using protein scaffold-directed assembly. Using the engineered yeast as artificial antigen presenting cells, we observed that the T cell activation threshold is determined by a minimum global pMHC surface density and independent of pMHC valency. Further, we found that T cell activation is maximized when pMHC and ICAM-1 are coassembled with a presentation ratio of 15% to 85%, respectively. In addition to increasing the magnitude of T cell activation, coassembly of 85% ICAM-1 enhanced T cell sensitivity to antigen by 6-fold. Taken together, these results suggest that adhesion molecules like ICAM-1 play an especially important role in 3D antigen presentation, as they maintain productive intercellular contacts necessary for T cell activation. As a result, the stoichiometric ratio between adhesion and stimulatory molecules should be carefully considered when designing future 3D antigen presenting systems. Finally, we believe the platform technology described here has applications beyond T cell antigen presentation, as it can be used for nanoscale patterning of any proteins of interest on any surfaces of interest.

METHODS

Design of pMHC, ICAM-1, and Cohesin Scaffolds. Recombinant pMHC fusion proteins were assembled by first isolating the extracellular domains of HLA-DRA (UniProt: P01903, residues 26−216) and HLA-DRB1*01:01 (UniProt: P04229, residues 30−227). The leucine zipper dimerization motifs Fos and Jun were fused to the C-terminus of the extracellular DRA and DRB1 chains, respectively, in lieu of the native transmembrane domains as described.[66] A dockerin domain from *C. thermocellum* (UniProt: A3DH67, residues 673−741) was fused to the C-terminus of the DRA construct *via* a 6X-Histidine tag. Two forms of the DRB1 chain were engineered. One DRB1*01:01 construct was fused to the invariant chain $CLIP_{87-101}$ peptide *via* a cleavable thrombin linker as described,[67] and one DRB1*01:01 construct was fused to the well-characterized influenza antigen $HA_{306-318}$ *via* the same cleavable thrombin linker. The C-termini of both DRB1*01:01 constructs were fused to a 6X-Histidine tag for purification and detection. The N-terminus of each dimeric chain was fused to the baculovirus gp64 signal peptide and

DOI: 10.1021/acssynbio.8b00119
ACS Synth. Biol. 2018, 7, 1629−1639

ligated into separate baculovirus transfer vectors pAcGP67A (BaculoGold Baculovirus Expression System, Pharmingen BD Biosciences, San Jose, CA). The integrity of each DNA sequence was confirmed using Sanger sequencing.

The murine intercellular adhesion molecule 1 (ICAM-1) was designed similarly. The DNA sequence coding the extracellular domain of ICAM-1 (UniProt: P13597, residues 28−485) was fused to the same *C. thermocellum* dockerin as DRA *via* a 6X-Histidine tag for purification and detection. The N-terminus of the ICAM-1 was fused to the baculovirus gp64 signal peptide and ligated into the baculovirus transfer vector pFastBac1 (Bac-to-Bac Baculovirus Expression Systems, Life Technologies). Separate baculovirus expression systems were used for pMHC and ICAM-1 because of the discontinuation of the BaculoGold-linearized baculovirus DNA. The difference did not affect protein expression.

Protein scaffolds were designed by recombining the sequences coding for the first three cohesins of the CipA cellulosome from *C. thermocellum*. Soluble protein scaffolds are denoted with the prefix "s"APC, and yeast-displayed scaffolds are denoted with the prefix "y"APC. sAPC1/yAPC1 consisted of Coh1 (UniProt: Q06851, residues 29−182); sAPC2/yAPC2 consisted of Coh1 and Coh2 (UniProt: Q06851, residues 29−322), and sAPC3/yAPC3 consisted of Coh1, Coh2, and Coh3 (UniProt: Q06851, residues 29−183 and residues 560−704). sAPC4/yAPC4 and sAPC5/yAPC5 contained the sAPC3 sequence fused to additional cohesins through a G−S−S-S linker (sAPC4: Coh1, Coh2, Coh3, and Coh1; sAPC5 Coh1, Coh2, Coh3, and Coh1, Coh2). All soluble protein scaffolds were ligated into the bacteria expression plasmid pET28a (Novagen) with a kanamycin resistance selectable marker. Yeast-displayed scaffolds were ligated into a modified form of the yeast surface display plasmid pYD1 (Invitrogen) with ampicillin resistance and tryptophan auxotrophic selectable markers and fused to an N-terminal Aga2 domain and a C-terminal V5 epitope tag for detection. All plasmids were propagated in the *E. coli* strain *Mach1*. All plasmids were sequenced using Sanger DNA sequencing for verification.

Baculovirus Transfection and pMHC, ICAM-1 Purification. *Spodoptera frugiperda* (SF9) insect cells were cotransfected with either the DRA or DRB1 baculovirus transfer vectors and linearized Baculovirus DNA (Pharmingen BD BaculoGold Biosciences, San Jose, CA) using Cellfectin II (Invitrogen) according to the manufacturer's protocol. The recombinant DRA and DRB1 baculoviruses generated from transfection were amplified separately in SF9 cells to create high-titer P1 viral stocks. pMHC was expressed by coinfecting High-Five cells at a density of 2.0 M/mL with equal volumes of high-titer DRA and DRB1 baculovirus stocks. Multiplicity of infection was optimized as described.[39] Recombinant pMHC was harvested after 72 h and purified using affinity chromatography with Ni-NTA beads according to the manufacturer's protocol (Qiagen). The ICAM-1 baculovirus transfer vector was transformed into the *E. coli* strain DH10Bac (Bac-to-Bac Baculovirus Expression Systems, Life Technologies). Bacmid recombination was established *via* blue/white colony screening and PCR recombination checks as described in the manufacturer's protocol. Recombinant baculovirus DNA was purified using a PureLink HiPure Plasmid miniprep kit (Invitrogen). ICAM-1 bacmid was used to transfect SF9 cells with Cellfectin II. The recombinant baculovirus generated from transfection was amplified in SF9 cells to obtain a high-titer P1 baculovirus stock. ICAM-1 was expressed by infecting High-Five cells at a density of 2.0 M/mL with high-titer ICAM-1 baculovirus stock. Recombinant ICAM-1 was purified in the same way as pMHC. SDS-PAGE analysis was performed to verify protein purity (Figure S7B).

Scaffold Purification and Scaffold-Directed Protein Complex Assembly. Plasmids coding for the soluble protein scaffolds were used to transform the *E. coli* strain BL21. Soluble protein scaffold expression was induced by addition of 0.1 mM IPTG in LB media when the BL21 culture reached an OD600 between 0.6 and 0.8. The induced BL21 were cultured for 16 h at 16 °C. Soluble protein scaffold was harvested by lysing the BL21 *via* sonication and performing affinity chromatography on the lysate using a 5 mL HisTrap column (GE Healthcare Life Sciences). The purified soluble protein scaffolds were analyzed using SDS-PAGE (Figure 2a) to verify protein purity.

For verifying the scaffold-directed assembly of recombinant dockerin-fused pMHC, ∼1.0 μg of each soluble protein scaffold construct (sAPC1−sAPC5) was incubated with excess pMHC in 50 mM Na_3PO_4 at 30 °C over 2 h. pMHC was added stepwise every 30 min over the 2 h incubation time. Complex formation was assessed by native-PAGE analysis. Briefly, the protein complexes were run on an 8% Tris-Glycine gel at 130 V for 2 h 15 min and stained using SimplyBlue SafeStain. Protein complex formation was assessed by observing a total shift of the soluble protein scaffold band.

Plasmids coding for yeast-displayed scaffolds were used to transform the *S. cerevisiae* strain EBY100. Transformants were selected by plating on tryptophan-dropout media. Transformed yeast were cultured to an OD600 of 4.0 in tryptophan-dropout media, and then scaffold expression was induced by transferring the yeast to galactose-rich media for 48 h at 20 °C. After induction, 500,000 of each yAPC (yAPC1−yAPC5) were incubated with excess pMHC in 0.5% bovine serum albumin (BSA) at 4 °C overnight. The yAPC were then washed twice with 0.5% BSA and costained with anti-His conjugated to PE (BioLegend) and anti-V5 conjugated to Alexa Fluor 647 (Invitrogen) for 1 h. The costained cells were then analyzed using flow cytometry. pMHC valency was determined by analyzing the ratio of pMHC (His) to scaffold (V5) median fluorescence intensities.

Fluorescent-Activated Cell Sorting. yAPC1−yAPC5 were prepared for FACS by initial fixation with 0.1% paraformaldehyde (PFA) for 15 min at room temperature. Fixation did not affect pMHC loading or T cell response. After fixation, the yAPC were washed 3 times with 0.5% BSA and then loaded with excess pMHC in 100 μL of 0.5% BSA at 4 °C overnight. The yAPC were washed 3× with 0.5% BSA, stained with Alexa Fluor 647-conjugated anti-His (clone AD1.1.10, BioRad Antibodies) for 1 h at room temperature, and resuspended in 1 mL of 0.5% BSA for FACS. The fluorophore-to-protein ratio (F/P) of the anti-His antibody was 3.1 and was provided by the manufacturer. Sorting was performed using a MoFlo Astrios (Beckman Coulter Life Sciences, Indianapolis, IN) cell sorter. Briefly, three or four gates were drawn based on distinct pMHC surface densities (as determined by the anti-His staining), and yAPC1−yAPC5 cells were sorted using these gates. The median fluorescence intensity was converted into median pMHC per cell using Quantum Alexa Fluor 647 Fluorescence Quantitation Beads (Bangs Laboratories, Fishers, IN). The uniformity of the sorted yAPC populations was confirmed by analyzing a fraction of the sorted yAPC using flow cytometry. For activation experiments requiring lower pMHC surface density than possible through

DOI: 10.1021/acssynbio.8b00119
ACS Synth. Biol. 2018, 7, 1629−1639

standard induction, yAPC were pretreated with 0.1−0.5 mM TCEP for 10 min at room temperature. This mild TCEP treatment decreased the number of surface-displayed scaffolds by reducing a fraction of the Aga1-Aga2 disulfide bonds anchoring each scaffold to the yeast cell surface. Cells were washed thoroughly with 0.5% BSA following TCEP treatment and then treated as described previously.

FACS involving pMHC-ICAM-1 coassembly was performed by first fixing yAPC1, yAPC3, and yAPC5 with 0.1% PFA for 10 min at room temperature. Following fixation, each yAPC was loaded with 85% ICAM-1 and 15% pMHC in 100 μL of 0.5% BSA at 4 °C overnight. The display ratio of 85% ICAM-1 and 15% pMHC was confirmed by staining a small fraction of each yAPC for ICAM-1 (clone YN1/1.7.4 BioLegend) and analyzing the samples using flow cytometry. ICAM-1 and pMHC loaded yAPC1, yAPC3, and yAPC5 were then washed and stained for both ICAM-1 and pMHC with Alexa Fluor 647-conjugated anti-His (clone AD1.1.10, BioRad Antibodies) and sorted and characterized in the same way as yAPC presenting pMHC alone.

T Cell Activation. T cell activation assays were performed in 96 well tissue culture plates at 37 °C and 5% CO_2. Activation plates were blocked prior to activation with 1% BSA overnight at 4 °C to minimize nonspecific immobilization of pMHC during activation. Murine HA1.7 T cell hybridoma[68] were cultured to a density of 2.0 M/mL in IMDM (Invitrogen) supplemented with 10% fetal bovine serum for activation. Once at this density, 200,000 HA1.7 T cells were applied to the activation wells in 200 μL of IMDM. In experiments involving sorted yAPC, 100,000 yAPC were used for activation. In experiments involving immobilization of pMHC for activation, pMHC was immobilized overnight at 4 °C in 1% BSA. In experiments involving sAPC-pMHC complexes for activation, the sAPC-pMHC were assembled 2 h prior to activation in 1% BSA in a volume of ∼7 μL and added to 200 μL of IMDM for activation. The activation supernatant was collected after 18 ± 2 h and analyzed using Ready-Set-Go IL-2 ELISA (eBiosciences, San Diego, CA) according to the manufacturer's protocol. The ELISA plate was developed for 10 min, and the IL-2 secretion was measured by recording the absorbance at 650 nm (A650). For ensuring consistency between experiments, a T cell activation index was calculated by dividing the A650 from activation wells by the A650 of the unstimulated controls. Thus, activation index indicates the multiple of IL-2 secretion over unstimulated T cells.

Regression Equations for T Cell Activation. T cell activation index was plotted against the average scaffold spacing for each yAPC construct. For each yAPC data set, activation index and scaffold spacing were logarithmically transformed and fitted using linear regression with a fixed slope of −2. The regression equations thus provided a valency-dependent constant for each yAPC curve. T cell activation thresholds were then calculated by solving for a scaffold spacing that corresponded to a T cell activation index of 1.0 for each yAPC. The scaffold spacing thresholds were then used to calculate the corresponding pMHC surface density to determine the global pMHC density thresholds for each yAPC. For pMHC-ICAM-1 coassembly experiments, the regression equation for T cell activation vs pMHC surface density was determined by logarithmically transforming the values for pMHC surface density and performing linear regression on the transformed data set. The minimum pMHC surface density requirement for measurable T cell IL-2 secretion was found by finding the pMHC surface density that corresponded to a T cell activation index of 1.0.

Statistical Analysis. Statistical analysis was performed using the Student's t test. All error bars are representative of the mean ± standard deviation of triplicate experiments unless otherwise noted. $*P < 0.05$, $**P < 0.01$, $***P < 0.001$.

■ ASSOCIATED CONTENT

Supporting Information

The Supporting Information is available free of charge on the ACS Publications website at DOI: 10.1021/acssynbio.8b00119.

yAPC, pMHC, and ICAM-1 fusion protein designs, yAPC-pMHC assembly schematic, pMHC and ICAM-1 binding affinity assays, pMHC-loaded yAPC characterization, pMHC-ICAM-1 coassembly characterization, and T cell activation with yAPC presenting pMHC-ICAM-1 coassemblies (PDF)

■ AUTHOR INFORMATION

Corresponding Author

*E-mail: feiwenum@umich.edu.

ORCID

Fei Wen: 0000-0001-7970-4796

Author Contributions

F.W. conceived and supervised the project and assisted in writing the manuscript. M.R.S. designed and performed all experiments and wrote the manuscript. S.V.T. helped with the expression of the pMHC protein. All authors read and revised the manuscript.

Notes

The authors declare no competing financial interest.

■ ACKNOWLEDGMENTS

The authors are grateful for the financial support by the National Science Foundation (NSF) under grant nos. 1511720, 1645229, and CAREER Award 1653611. The authors thank all group members from Dr. Fei Wen's lab for their constructive feedback. The authors also thank the University of Michigan Flow Cytometry Core for assistance with FACS and A. Mady and Z. Nikolovska-Coleska for assistance with SPR experiments.

■ REFERENCES

(1) Rosenberg, S. A. (2012) Raising the Bar: The Curative Potential of Human Cancer Immunotherapy. *Sci. Transl. Med. 4*, 127ps8−127ps8.

(2) The Lancet (2017) CAR T-cells: an exciting frontier in cancer therapy. *Lancet 390*, 1006.

(3) Kamphorst, A. O., and Ahmed, R. (2013) CD4 T-cell immunotherapy for chronic viral infections and cancer. *Immunotherapy 5*, 975−987.

(4) Han, S., Latchoumanin, O., Wu, G., Zhou, G., Hebbard, L., George, J., and Qiao, L. (2017) Recent clinical trials utilizing chimeric antigen receptor T cells therapies against solid tumors. *Cancer Lett. 390*, 188−200.

(5) Heslop, H. E., Ng, C. Y. C., Li, C., Smith, C. A., Loftin, S. K., Krance, R. A., Brenner, M. K., and Rooney, C. M. (1996) Long−term restoration of immunity against Epstein−Barr virus infection by adoptive transfer of gene−modified virus−specific T lymphocytes. *Nat. Med. 2*, 551−555.

(6) Chen, L., and Flies, D. B. (2013) Molecular mechanisms of T cell co-stimulation and co-inhibition. *Nat. Rev. Immunol. 13*, 227−242.

DOI: 10.1021/acssynbio.8b00119
ACS Synth. Biol. 2018, 7, 1629−1639

(7) Kinnear, G., Jones, N. D., and Wood, K. J. (2013) Costimulation Blockade. *Transplantation 95*, 527−535.
(8) Manz, B. N., Jackson, B. L., Petit, R. S., Dustin, M. L., and Groves, J. (2011) T-cell triggering thresholds are modulated by the number of antigen within individual T-cell receptor clusters. *Proc. Natl. Acad. Sci. U. S. A. 108*, 9089−94.
(9) Mossman, K., and Groves, J. (2007) Micropatterned supported membranes as tools for quantitative studies of the immunological synapse. *Chem. Soc. Rev. 36*, 46−54.
(10) Groves, J. T., and Dustin, M. L. (2003) Supported planar bilayers in studies on immune cell adhesion and communication. *J. Immunol. Methods 278*, 19−32.
(11) Mossman, K. D., Campi, G., Groves, J. T., and Dustin, M. L. (2005) Altered TCR signaling from geometrically repatterned immunological synapses. *Science 310*, 1191−1193.
(12) Irvine, D. J., and Doh, J. (2007) Synthetic surfaces as artificial antigen presenting cells in the study of T cell receptor triggering and immunological synapse formation. *Semin. Immunol. 19*, 245−54.
(13) Cai, H., Depoil, D., Palma, M., Sheetz, M. P., Dustin, M. L., and Wind, S. J. (2013) Bifunctional nanoarrays for probing the immune response at the single-molecule level. *J. Vac. Sci. Technol., B: Nanotechnol. Microelectron.: Mater., Process., Meas., Phenom. 31*, 6F902.
(14) Doh, J., and Irvine, D. J. (2006) Immunological synapse arrays: patterned protein surfaces that modulate immunological synapse structure formation in T cells. *Proc. Natl. Acad. Sci. U. S. A. 103*, 5700−5.
(15) Cai, H., Wolfenson, H., Depoil, D., Dustin, M. L., Sheetz, M. P., and Wind, S. J. (2016) Molecular Occupancy of Nanodot Arrays. *ACS Nano 10*, 4173−83.
(16) Deeg, J., Axmann, M., Matic, J., Liapis, A., Depoil, D., Afrose, J., Curado, S., Dustin, M. L., and Spatz, J. P. (2013) T cell activation is determined by the number of presented antigens. *Nano Lett. 13*, 5619−26.
(17) Matic, J., Deeg, J., Scheffold, A., Goldstein, I., and Spatz, J. P. (2013) Fine tuning and efficient T cell activation with stimulatory aCD3 nanoarrays. *Nano Lett. 13*, 5090−7.
(18) Delcassian, D., Depoil, D., Rudnicka, D., Liu, M., Davis, D. M., Dustin, M. L., and Dunlop, I. E. (2013) Nanoscale ligand spacing influences receptor triggering in T cells and NK cells. *Nano Lett. 13*, 5608−14.
(19) Cochran, J. R., Cameron, T. O., Stone, J. D., Lubetsky, J. B., and Stern, L. J. (2001) Receptor proximity, not intermolecular orientation, is critical for triggering T-cell activation. *J. Biol. Chem. 276*, 28068−74.
(20) Hammink, R., Mandal, S., Eggermont, L. J., Nooteboom, M., Willems, P. H. G. M., Tel, J., Rowan, A. E., Figdor, C. G., and Blank, K. G. (2017) Controlling T-Cell Activation with Synthetic Dendritic Cells Using the Multivalency Effect. *ACS omega 2*, 937−945.
(21) Bennett, N. R., Zwick, D. B., Courtney, A. H., and Kiessling, L. L. (2015) Multivalent Antigens for Promoting B and T Cell Activation. *ACS Chem. Biol. 10*, 1817−24.
(22) Motta, I., Lone, Y.-C., and Kourilsky, P. (1998) In vitro induction of naive cytotoxic T lymphocytes with complexes of peptide and recombinant MHC class I molecules coated onto beads: role of TCR/ligand density. *Eur. J. Immunol. 28*, 3685−3695.
(23) Irvine, D. J., Purbhoo, M. a., Krogsgaard, M., and Davis, M. M. (2002) Direct observation of ligand recognition by T cells. *Nature 419*, 845−9.
(24) Perica, K., Kosmides, A. K., and Schneck, J. P. (2015) Linking form to function: Biophysical aspects of artificial antigen presenting cell design. *Biochim. Biophys. Acta, Mol. Cell Res. 1853*, 781−790.
(25) Bosch, B., Heipertz, E. L., Drake, J. R., and Roche, P. A. (2013) Major histocompatibility complex (MHC) class II-peptide complexes arrive at the plasma membrane in cholesterol-rich microclusters. *J. Biol. Chem. 288*, 13236−13242.
(26) Schamel, W. W. A., and Alarcón, B. (2013) Organization of the resting TCR in nanoscale oligomers. *Immunol. Rev. 251*, 13−20.
(27) Kamalasanan, K., Jhunjhunwala, S., Wu, J., Swanson, A., Gao, D., and Little, S. R. (2011) Patchy, anisotropic microspheres with soft protein islets. *Angew. Chem., Int. Ed. 50*, 8706−8.
(28) Chen, B., Jia, Y., Gao, Y., Sanchez, L., Anthony, S. M., and Yu, Y. (2014) Janus particles as artificial antigen-presenting cells for T cell activation. *ACS Appl. Mater. Interfaces 6*, 18435−9.
(29) Verma, N. K., and Kelleher, D. (2017) Not Just an Adhesion Molecule: LFA-1 Contact Tunes the T Lymphocyte Program. *J. Immunol. 199*, 1213−1221.
(30) Zhang, H., Snyder, K. M., Suhoski, M. M., Maus, M. V., Kapoor, V., June, C. H., and Mackall, C. L. (2007) 4−1BB Is Superior to CD28 Costimulation for Generating CD8+ Cytotoxic Lymphocytes for Adoptive Immunotherapy. *J. Immunol. 179*, 4910−4918.
(31) Suhoski, M. M., Golovina, T. N., Aqui, N. a., Tai, V. C., Varela-Rohena, A., Milone, M. C., Carroll, R. G., Riley, J. L., and June, C. H. (2007) Engineering artificial antigen-presenting cells to express a diverse array of co-stimulatory molecules. *Mol. Ther. 15*, 981−8.
(32) Zeng, W., Su, M., Anderson, K. S., and Sasada, T. (2014) Artificial antigen-presenting cells expressing CD80, CD70, and 4−1BB ligand efficiently expand functional T cells specific to tumor-associated antigens. *Immunobiology 219*, 583−592.
(33) Hodge, J. W., Sabzevari, H., Yafal, A. G., Gritz, L., Lorenz, M. G., and Schlom, J. (1999) A triad of costimulatory molecules synergize to amplify T-cell activation. *Cancer Res. 59*, 5800−7.
(34) Tang, X.-Y., Sun, Y., Zhang, A., Hu, G.-L., Cao, W., Wang, D.-H., Zhang, B., and Chen, H. (2016) Third-generation CD28/4−1BB chimeric antigen receptor T cells for chemotherapy relapsed or refractory acute lymphoblastic leukaemia: a non-randomised, open-label phase I trial protocol. *BMJ. Open 6*, e013904.
(35) Li, Y., and Kurlander, R. J. (2010) Comparison of anti-CD3 and anti-CD28-coated beads with soluble anti-CD3 for expanding human T cells: Differing impact on CD8 T cell phenotype and responsiveness to restimulation. *J. Transl. Med. 8*, 104.
(36) Zappasodi, R., Di Nicola, M., Carlo-Stella, C., Mortarini, R., Molla, A., Vegetti, C., Albani, S., Anichini, A., and Gianni, A. M. (2008) The effect of artificial antigen-presenting cells with preclustered anti-CD28/-CD3/-LFA-1 monoclonal antibodies on the induction of ex vivo expansion of functional human antitumor T cells. *Haematologica 93*, 1523−34.
(37) Sun, F., Zhang, W.-B., Mahdavi, A., Arnold, F. H., and Tirrell, D. A. (2014) Synthesis of bioactive protein hydrogels by genetically encoded SpyTag-SpyCatcher chemistry. *Proc. Natl. Acad. Sci. U. S. A. 111*, 11269−11274.
(38) Wen, F., and Zhao, H. (2013) Construction and Screening of an Antigen-Derived Peptide Library Displayed on Yeast Cell Surface for CD4+ T Cell Epitope Identification, in *Immunoproteomics: Methods and Protocols* (Fulton, K. M., and Twine, S. M., Eds.), pp 245−264.
(39) Wen, F., Sethi, D. K., Wucherpfennig, K. W., and Zhao, H. (2011) Cell surface display of functional human MHC class II proteins: yeast display versus insect cell display. *Protein Eng., Des. Sel. 24*, 701−9.
(40) Boder, E. T., Bill, J. R., Nields, A. W., Marrack, P. C., and Kappler, J. W. (2005) Yeast surface display of a noncovalent MHC class II heterodimer complexed with antigenic peptide. *Biotechnol. Bioeng. 92*, 485−91.
(41) Smith, M. R., Khera, E., and Wen, F. (2015) Engineering Novel and Improved Biocatalysts by Cell Surface Display. *Ind. Eng. Chem. Res. 54*, 4021−4032.
(42) Boder, E. T., and Wittrup, K. D. (1997) Yeast surface display for screening combinatorial polypeptide libraries. *Nat. Biotechnol. 15*, 553−7.
(43) Gai, S. A., and Wittrup, K. D. (2007) Yeast surface display for protein engineering and characterization. *Curr. Opin. Struct. Biol. 17*, 467−73.
(44) Smith, S. N., Harris, D. T., and Kranz, D. M. (2015) Yeast Surface Display (Liu, B., Ed.).
(45) Wu, C. H., Mulchandani, A., and Chen, W. (2008) Versatile microbial surface-display for environmental remediation and biofuels production. *Trends Microbiol. 16*, 181−188.
(46) Gerngross, U. T., Romaniec, M. P., Kobayashi, T., Huskisson, N. S., and Demain, a L. (1993) Sequencing of a Clostridium thermocellum gene (cipA) encoding the cellulosomal SL-protein

DOI: 10.1021/acssynbio.8b00119
ACS Synth. Biol. 2018, 7, 1629−1639

reveals an unusual degree of internal homology. *Mol. Microbiol. 8*, 325−34.
(47) Wen, F., Sun, J., and Zhao, H. (2010) Yeast surface display of trifunctional minicellulosomes for simultaneous saccharification and fermentation of cellulose to ethanol. *Appl. Environ. Microbiol. 76*, 1251−60.
(48) Handelsman, T., Barak, Y., Nakar, D., Mechaly, A., Lamed, R., Shoham, Y., and Bayer, E. A. (2004) Cohesin-dockerin interaction in cellulosome assembly: a single Asp-to-Asn mutation disrupts high-affinity cohesin-dockerin binding. *FEBS Lett. 572*, 195−200.
(49) Stern, L. J., Brown, J. H., Jardetzky, T. S., Gorga, J. C., Urban, R. G., Strominger, J. L., and Wiley, D. C. (1994) Crystal structure of the human class II MHC protein HLA-DR1 complexed with an influenza virus peptide. *Nature 368*, 215−21.
(50) Hennecke, J., Carfi, A., and Wiley, D. C. (2000) Structure of a covalently stabilized complex of a human alphabeta T-cell receptor, influenza HA peptide and MHC class II molecule, HLA-DR1. *EMBO J. 19*, 5611−24.
(51) Day, C. L., Seth, N. P., Lucas, M., Appel, H., Gauthier, L., Lauer, G. M., Robbins, G. K., Szczepiorkowski, Z. M., Casson, D. R., Chung, R. T., Bell, S., Harcourt, G., Walker, B. D., Klenerman, P., and Wucherpfennig, K. W. (2003) Ex vivo analysis of human memory CD4 T cells specific for hepatitis C virus using MHC class II tetramers. *J. Clin. Invest. 112*, 831−42.
(52) Cochran, J. R., Cameron, T. O., and Stern, L. J. (2000) The Relationship of MHC-Peptide Binding and T Cell Activation Probed Using Chemically Defined MHC Class II Oligomers. *Immunity 12*, 241−250.
(53) Ma, Z., Sharp, K. a., Janmey, P. a., and Finkel, T. H. (2008) Surface-anchored monomeric agonist pMHCs alone trigger TCR with high sensitivity. *PLoS Biol. 6*, e43.
(54) Xie, J., Huppa, J. B., Newell, E. W., Huang, J., Ebert, P. J. R., Li, Q.-J., and Davis, M. M. (2012) Photocrosslinkable pMHC monomers stain T cells specifically and cause ligand-bound TCRs to be "preferentially" transported to the cSMAC. *Nat. Immunol. 13*, 674−680.
(55) Wang, X. X., and Shusta, E. V. (2005) The use of scFv-displaying yeast in mammalian cell surface selections. *J. Immunol. Methods 304*, 30−42.
(56) Lillemeier, B. F., Mörtelmaier, M. A., Forstner, M. B., Huppa, J. B., Groves, J. T., and Davis, M. M. (2010) TCR and Lat are expressed on separate protein islands on T cell membranes and concatenate during activation. *Nat. Immunol. 11*, 90−96.
(57) Dustin, M. L., and Springer, T. A. (1989) T-cell receptor cross-linking transiently stimulates adhesiveness through LFA-1. *Nature 341*, 619−24.
(58) Lollo, B. a., Chan, K. W., Hanson, E. M., Moy, V. T., and Brian, a a. (1993) Direct evidence for two affinity states for lymphocyte function-associated antigen 1 on activated T cells. *J. Biol. Chem. 268*, 21693−700.
(59) Mueller, K. L., Daniels, M. A., Felthauser, A., Kao, C., Jameson, S. C., and Shimizu, Y. (2004) Cutting edge: LFA-1 integrin-dependent T cell adhesion is regulated by both ag specificity and sensitivity. *J. Immunol. 173*, 2222−6.
(60) Comrie, W. A., Li, S., Boyle, S., and Burkhardt, J. K. (2015) The dendritic cell cytoskeleton promotes T cell adhesion and activation by constraining ICAM-1 mobility. *J. Cell Biol. 208*, 457−73.
(61) Suzuki, J., Yamasaki, S., Wu, J., Koretzky, G. A., and Saito, T. (2007) The actin cloud induced by LFA-1-mediated outside-in signals lowers the threshold for T-cell activation. *Blood 109*, 168−75.
(62) Wülfing, C., Sjaastad, M. D., and Davis, M. M. (1998) Visualizing the dynamics of T cell activation: intracellular adhesion molecule 1 migrates rapidly to the T cell/B cell interface and acts to sustain calcium levels. *Proc. Natl. Acad. Sci. U. S. A. 95*, 6302−6307.
(63) Zuckerman, L. A., Pullen, L., and Miller, J. (1998) Functional consequences of costimulation by ICAM-1 on IL-2 gene expression and T cell activation. *J. Immunol. 160*, 3259−68.
(64) Verma, N. K., Fazil, M. H. U. T., Ong, S. T., Chalasani, M. L. S., Low, J. H., Kottaiswamy, A., Kizhakeyil, A., Kumar, S., Panda, A. K., Freeley, M., Smith, S. M., Boehm, B. O., and Kelleher, D. (2016) LFA-1/ICAM-1 Ligation in Human T Cells Promotes Th1 Polarization through a GSK3β Signaling-Dependent Notch Pathway. *J. Immunol. 197*, 108−118.
(65) Smits, H. H., de Jong, E. C., Schuitemaker, J. H. N., Geijtenbeek, T. B. H., van Kooyk, Y., Kapsenberg, M. L., and Wierenga, E. A. (2002) Intercellular adhesion molecule-1/LFA-1 ligation favors human Th1 development. *J. Immunol. 168*, 1710−6.
(66) Kalandadze, A., Galleno, M., Foncerrada, L., Strominger, J. L., and Wucherpfennig, K. W. (1996) Expression of Recombinant HLA-DR2Molecules. *J. Biol. Chem. 271*, 20156−20162.
(67) Jang, M.-H., Seth, N. P., and Wucherpfennig, K. W. (2003) Ex Vivo Analysis of Thymic CD4 T Cells in Nonobese Diabetic Mice with Tetramers Generated from I-Ag7/Class II-Associated Invariant Chain Peptide Precursors. *J. Immunol. 171*, 4175−4186.
(68) Boen, E., Crownover, a R., McIlhaney, M., Korman, a J., and Bill, J. (2000) Identification of T Cell Ligands in a Library of Peptides Covalently Attached to HLA-DR4. *J. Immunol. 165*, 2040−2047.

DOI: 10.1021/acssynbio.8b00119
ACS Synth. Biol. 2018, 7, 1629−1639